

Tunable and Enhanced Rashba Spin-Orbit Coupling in Iridate-Manganite Heterostructures

T. S. Suraj^{1,2,*}, Ganesh Ji Omar^{3,4,*}, Hariom Jani^{4,6}, Muhammad Mangattuchali Juvaidd^{1,3,4}, Sonu Hooda⁴, Anindita Chaudhuri⁵, Andriwo Rusydi^{3,5}, Kanikrishnan Sethupathi², Thirumalai Venkatesan^{3,4,6,7,8}, Ariando Ariando^{3,4,6,†} and Mamidanna Sri Ramachandra Rao^{1‡}

¹ Department of Physics, Nano Functional Materials Technology Center,

Material Science Research Center, IIT Madras, India 600036

² Low Temperature Physics Lab, Department of Physics,

Indian institute of Madras, Chennai, India 600036

³ Department of Physics, National University of Singapore, Singapore 117542, Singapore

⁴ NUSNNI-NanoCore, National University of Singapore, Singapore 117411

⁵ Singapore Synchrotron Light Source, National University of Singapore, 5 Research Link, Singapore 117603, Singapore

⁶ National University of Singapore Graduate School for Integrative Sciences and Engineering (NGS), University Hall, 21 Lower Kent Ridge Road, Singapore 119077

⁷ Department of Materials Science and Engineering, National University of Singapore, Singapore 117575, Singapore and

⁸ Department of Electrical and Computer Engineering, National University of Singapore, Singapore 117576, Singapore

(Dated: October 11, 2021)

Tailoring spin-orbit interactions and Coulomb repulsion are the key features to observe exotic physical phenomena such as magnetic anisotropy and topological spin texture at oxide interfaces. Our study proposes a novel platform for engineering the magnetism and spin-orbit coupling at $\text{LaMnO}_3/\text{SrIrO}_3$ ($3d$ - $5d$ oxide) interfaces by tuning the LaMnO_3 growth conditions which controls the lattice displacement and spin-correlated interfacial coupling through charge transfer. We report on a tunable and enhanced interface-induced Rashba spin-orbit coupling and Elliot-Yafet spin relaxation mechanism in $\text{LaMnO}_3/\text{SrIrO}_3$ bilayer with change in the underlying magnetic order of LaMnO_3 . We also observed enhanced spin-orbit coupling strength in $\text{LaMnO}_3/\text{SrIrO}_3$ compared to previously reported SrIrO_3 layers. The X-Ray spectroscopy measurement reveals the quantitative valence of Mn and their impact on charge transfer. Further, we performed angle-dependent magnetoresistance measurements, which show signatures of magnetic proximity effect in SrIrO_3 while reflecting the magnetic order of LaMnO_3 . Our work thus demonstrates a new route to engineer the interface induced Rashba spin-orbit coupling and magnetic proximity effect in $3d$ - $5d$ oxide interfaces which makes SrIrO_3 an ideal candidate for spintronics applications.

I. INTRODUCTION

The combination of artificially layered complex oxides in heterostructures opens the possibility of realizing novel functional properties from the strong interplay among charge, spin, orbit and lattice degrees of freedom which might be absent in the constituent oxide layers. Moreover, the interfacial effects mediated through charge transfer between oxide layers play a significant role in tuning the interface physics and its resultant properties [1–5]. Among oxides, there is a surge in research interest for combinations of $3d$ - $5d$ oxide interfaces for exploring various novel phenomena, such as manipulation of spin-orbit coupling that has potential applications in spintronics memory devices [6–8]. Among $5d$ oxide materials, iridates are the most exciting due to the combination of large intrinsic spin-orbit coupling (interaction strength; ξ) and their tunable coulombic correlations (interaction strength; U) [9]. The strong spin-orbit coupling in $5d$

orbital state splits the t_{2g} levels due to crystal field into a fully filled $J_{eff} = \frac{3}{2}$ quartet and the $J_{eff} = \frac{1}{2}$ doublet having a single electron (hole) forming a half-filled band. Depending on the interaction strength (U), an iridate system can become a Mott insulator, or it can be driven to have a metallic/semi-metallic ground state [10–12]. Perovskite SrIrO_3 can be epitaxially grown over various transition metal oxides (TMO), and its semi-metallicity can be tuned by compressive strain and reduced dimensionality, which makes it an ideal choice as $5d$ oxide layers in $3d$ - $5d$ heterostructures [13–15].

On the other hand, LaMnO_3 is the parent compound for manganite, containing the $3d$ element Mn, which is an A-type antiferromagnetic insulator in bulk and could behave like a ferromagnet in epitaxial thin films due to vacancies or epitaxial strain [16–18]. Our earlier studies demonstrate the origin of ferromagnetism in $\text{LaMnO}_3/\text{SrTiO}_3$ heterostructures by mapping the magnetic domains which show long-range ferromagnetic ordering arising from electron doping at the $\text{LaMnO}_3/\text{SrTiO}_3$ due to polar catastrophe [19]. LaMnO_3 thin films grown under different deposition oxygen partial pressures ($p\text{O}_2$) have also been systematically studied by different groups with a variety of experimental techniques

* Authors contributed equally

† ariando@nus.edu.sg

‡ msrrao@iitm.ac.in

such as X-ray Absorption Spectroscopy (XAS), X-ray Magnetic Circular Dichroism (XMCD) and Transmission Electron Microscopy-Electron Energy Loss Spectroscopy (TEM-EELS) [18–23]. Roqueta *et al.* reported tunability of strain-controlled ferromagnetism in LaMnO_3 during growth by varying the background $p\text{O}_2$ that resulted in a rich magnetic phase diagram. However, the oxygen non-stoichiometry creates an imbalance in Mn valence states by charge ordering, which induces double exchange mediated ferromagnetism in LaMnO_3 [20]. This aspect of oxygen non-stoichiometry tuning to control spin-orbit interactions via a $3d$ - $5d$ interface has hitherto not been explored.

The interaction of transition metal oxides with SrIrO_3 exhibited very interesting properties, for example, tuning magnetic anisotropy in $\text{La}_{1-x}\text{Sr}_x\text{MnO}_3/\text{SrIrO}_3$ superlattices through octahedral rotation [24, 25] and inducing metal-insulator transition in LaNiO_3 by charge transfer from SrIrO_3 [26]. Novel magnetic phases such as spin-glass and skyrmions in $\text{SrRuO}_3/\text{SrIrO}_3$ superlattices were also reported [27]. The interfacial charge transfer driven phenomena like the emergence of magnetism in $\text{SrIrO}_3/\text{SrMnO}_3$ superlattices [1, 28] and interfacial re-entrant spin/super spin-glass state has been reported recently in $\text{LaMnO}_3/\text{SrIrO}_3$ bilayer [29].

In this work, we demonstrate the influence of LaMnO_3 layer on magneto-transport and spin-orbit coupling properties at the SrIrO_3 interface where LaMnO_3 growth condition plays a major role. Our magneto-transport measurements show a tunable and enhanced Rashba spin-orbit coupling at the interface with varying magnetic behaviour of LaMnO_3 . In addition, X-ray photoelectron spectroscopy (XPS) measurements indicates different fraction of Mn^{3+} and Mn^{4+} valence states in LaMnO_3 grown at different oxygen partial pressures, this affects the spin-orbit coupling related parameters at $\text{LaMnO}_3/\text{SrIrO}_3$ interface. Also, interfacial charge transfer from Ir^{4+} to Mn^{3+} and Mn^{4+} from growth variation has not been reported at a $3d$ - $5d$ interface, where as individual (Mn^{3+}) $\text{LaMnO}_3/\text{SrIrO}_3$ [29] and (Mn^{4+}) $\text{SrMnO}_3/\text{SrIrO}_3$ interfaces charge transfer have been reported earlier [1, 28].

Spin Hall magnetoresistance (SMR) has become a versatile tool to probe the nature of magnetic interfaces [30, 31]. In our case, LaMnO_3 is a magnetic layer and SrIrO_3 is a metallic oxide with large spin-orbit coupling [31]. Although SrIrO_3 is the best choice for spin-transport studies due to low charge conductivity and large spin-orbit coupling, it has not been thoroughly explored through electrical transport measurements [32]. The angle-dependent magnetoresistance (ADMR) measurements showed signatures of magnetic proximity effect (MPE) in SrIrO_3 , which is reflected in ADMR magnitude as well. Our study provides a new platform for tuning interfacial effects in TMO heterostructures by interface modifications which may have an impact on designing spintronic devices with an emerging $5d$ quantum material.

II. RESULTS AND DISCUSSION

LaMnO_3 thin films were grown on (001) oriented $(\text{LaAlO}_3)_{0.3}(\text{Sr}_2\text{TaAlO}_6)_{0.7}$ (LSAT) substrates by pulsed laser deposition (PLD) in order to rule out the possibility of polar catastrophe and minimize lattice mismatch. LP-LMO denotes 10 nm thick LaMnO_3 grown at low $p\text{O}_2$ (37.5×10^{-3} mTorr), similarly HP-LMO denotes 10 nm thick LaMnO_3 grown at high $p\text{O}_2$ (37.5 mTorr). The $\text{LaMnO}_3/\text{SrIrO}_3$ bilayers with 5 nm thick SrIrO_3 deposited on top of HP- and LP- LMO under similar conditions (deposition $p\text{O}_2 = 100$ mTorr) are labelled as LP-/HP- LMO-SIO respectively, the detailed growth-related procedure is given in supplementary information Figure S1. The quality of PLD grown LP/HP-LMO samples are confirmed by Atomic Force Microscopy (AFM) and X-ray Diffraction (XRD) studies (Figure S2 and S3).

The electrical and magnetotransport properties of the samples are investigated using PPMS transport measurement system (more details are given in Supplementary Information). The temperature-dependent resistivity $\rho(T)$ is shown in the Fig. 1a. To rule out the possibility of electrical conduction channels through LP-/HP- LMO, we have measured resistivity of individual layers grown on LSAT substrates which were highly resistive compared to the SrIrO_3 semimetallic layer, as shown in the supplementary Figure S4. The temperature-dependent behaviour of magnetization (field cooling; FC) measured at 500 Oe of these bilayer samples are also shown in Fig. 1b. The first change of slope in the ρ vs T plot of the HP-LMO-SIO sample was found to be around 50 K (defined as T_1 , in Fig. 1a), which corresponds to weak anti-localization to weak localization crossover usually found in SrIrO_3 thin films [34]. The second change of slope near 210 K (defined as T_2), which corresponds to the ferromagnetic to paramagnetic transition of LaMnO_3 , as shown in Figure 1b. Similarly, the change of slope near 120 K (defined as T_3) in electrical transport measurements (see Fig. 1a) also corresponds to Curie temperature (T_C) of the LP-LMO layer (see Fig. 1b) in the magnetic measurements. A clear shift in the T_C as well as the magnitude of the magnetic moment in both the samples are consistent with earlier reports, ascertaining that the disproportion of Mn^{3+} and Mn^{4+} drives LaMnO_3 layer to different magnetic order [22, 23]. The oxygen gas atmosphere during the deposition allows oxygen to be absorbed into the lattice, thereby enhancing the formation of Mn^{4+} ions promoting double exchange mediated ferromagnetic ordering in epitaxial HP-LMO thin films [20, 22, 23]. When the $p\text{O}_2$ during LaMnO_3 deposition decreases, this enhances formation of increased Mn^{3+} which has smaller magnetic moment compared to Mn^{4+} the LaMnO_3 layer evolves to an antiferromagnetic ground state. To quantify Mn^{3+} and Mn^{4+} , we have performed X-ray photoelectron spectroscopy (XPS) measurements on HP- and LP- LMO samples (see supplementary Figure S5), which is a surface-sensitive technique. XPS results are in agreement with earlier reports of in-

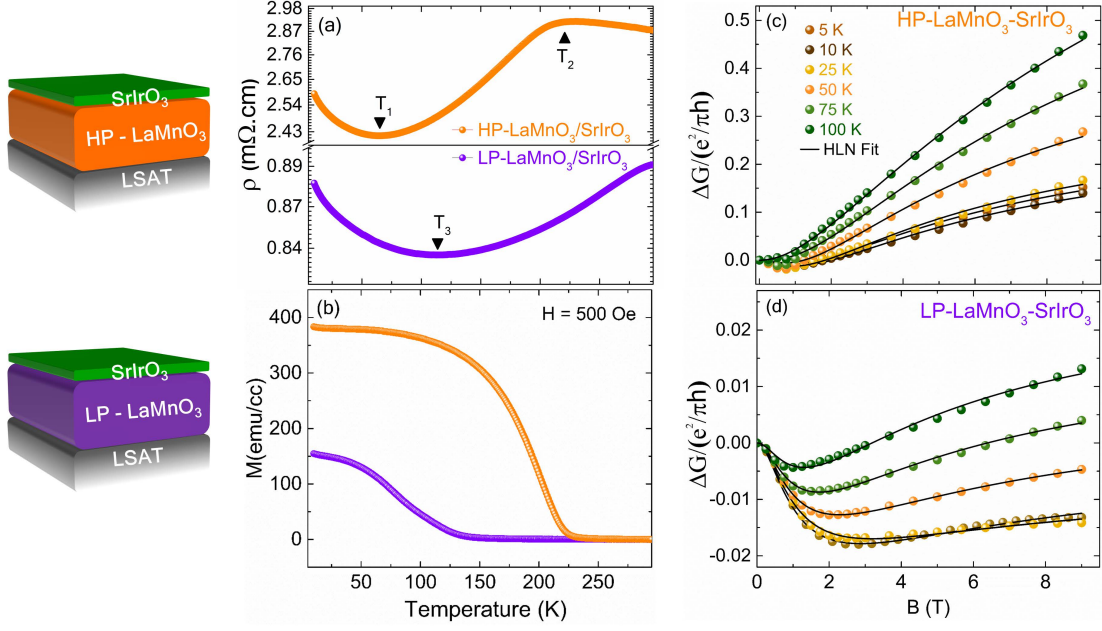


FIG. 1. Schematic image of the layered structure of LaMnO_3 deposited at 37.5 mTorr (HP-LMO-SIO) and 37.5×10^{-3} mTorr (LP-LMO-SIO) bilayer samples (left). (a) Temperature dependence of resistivity (ρ) and (b) magnetization (M) at an applied magnetic field of 500 Oe in Field cooled (FC) protocol are demonstrated in (a) and (b) respectively for HP- and LP- LMO-SIO bilayer. (c) and (d) experimental magnetoconductance (ΔG) data (closed colored symbols) as a function of magnetic field (B) \perp interface; measured for different temperatures fitted (solid black curve) by the Hikami-Larkin-Nagaoka equation for HP- and LP- LMO-SIO samples respectively.

creased Mn^{4+} content in HP-LMO samples and lower content of Mn^{4+} in LP-LMO samples. Also, to verify the oxygen non-stoichiometry and La/Mn ratio, we have carried out Rutherford backscattering spectroscopy (RBS) in LaMnO_3 thin films grown at different $p\text{O}_2$. The RBS data (Figure S6) shows that the HP-/LP-LMO samples are nearly stoichiometric, see supplemental material Figure S6(b). The oxygen content in the LaMnO_3 thin films are roughly estimated, which has been found to increase for the HP-LMO sample compared to that of the LP-LMO, as shown in supplemental material Figure S6(c).

To further understand the electronic transport behaviour and electron spin relaxation mechanism, magnetotransport measurements were carried out on the bilayer samples at different temperatures as shown in Fig. 1c and d. The Magnetoconductance (MC) showed a negative to positive crossover which was dominant at low temperatures and this crossover trend becomes weaker with increase in temperature and vanishes near 100 K and 125 K for LP-/HP- LMO-SIO respectively. At low magnetic fields the negative MC

component is dominant, and at high magnetic fields the positive MC component is dominant. Negative MC (at temperatures below 10 K) reported in ultrathin SrIrO_3 films grown on compressively strained LSAT and STO substrates arises due to the competition between weak localization (WL) and strong spin-orbit coupling based weak anti-localization effects (WAL) [33]. Usually, from various reports, the crossover from negative to positive MC arises in ultrathin SrIrO_3 thin films in the temperature range of 7-10 K [13, 33, 34]. However, we observed a crossover in MC at low magnetic fields in the temperature range of 100 to 125 K for both HP- and LP- LMO-SIO, as shown in Fig. 1c and d. SrIrO_3 grown on HP- and LP- LMO show different temperature dependence in the crossover of MC from positive MC to negative MC. In addition, the shape of MC has also been found to change for both samples. To investigate this scenario in terms of spin-orbit coupling in the LP- and HP- LMO-SIO layer, we used Hikami-Larkin-Nagaoka (HLN) equation [35] to fit the MC data.

$$\frac{\Delta\sigma(B)}{G_0} = -\Psi\left(\frac{1}{2} + \frac{B_e}{B}\right) + \frac{3}{2}\Psi\left(\frac{1}{2} + \frac{B_i + B_{so}}{B}\right) - \frac{1}{2}\Psi\left(\frac{1}{2} + \frac{B_i}{B}\right) - \ln\left(\frac{B_i + B_{so}}{B_e}\right) - \frac{1}{2}\ln\left(\frac{B_i + B_{so}}{B}\right) \quad (1)$$

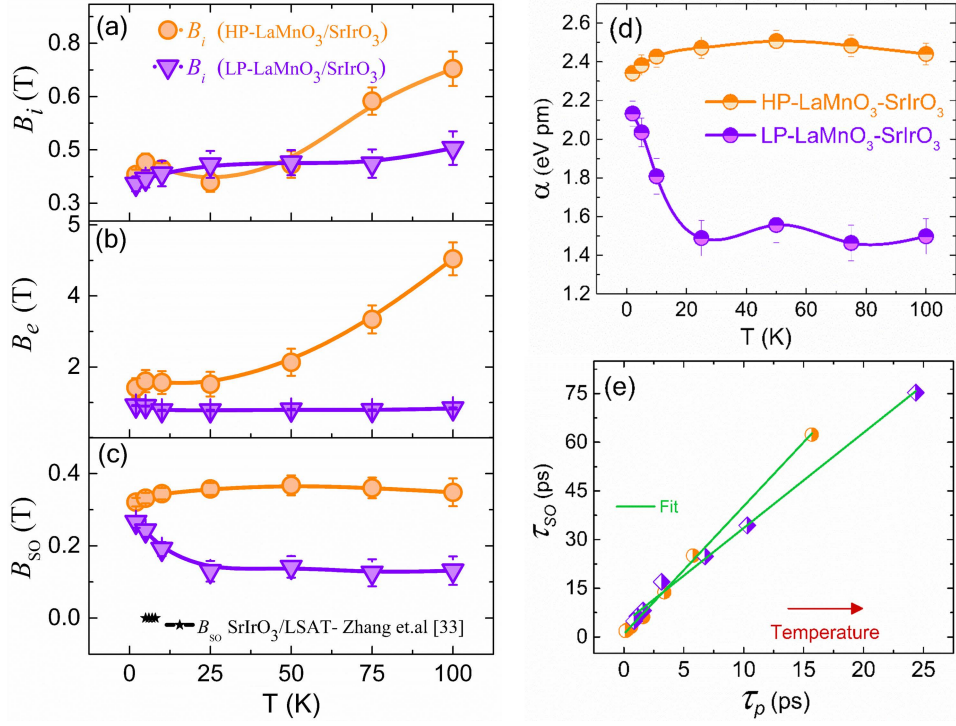


FIG. 2. Evolution of fitting parameters B_i (panel a), B_e (panel b) and B_{SO} (panel c) as a function of temperature for HP- and LP- LMO-SIO sample, also SrIrO₃/LSAT (001)[33] has also been plotted for comparison in (c). (d) Rashba spin-orbit coupling (α) extracted from B_{SO} values using Eqn.3 is shown as a function of temperature for HP and LP samples. (e) Spin relaxation timescale (τ_{so}) vs momentum scattering timescale (τ_p) dependency is consistent with the ElliotYafet mechanism for HP- and LP- LMO-SIO samples. Linear fit (solid green colour) where $\tau_{so} \propto \tau_p$.

In the Eq. (1) ψ is digamma function and G_0 is the universal conductance constant; 1.2×10^{-5} S. B_e , B_i and B_{so} represents effective fields of elastic, inelastic, and spin-orbit coupling induced scattering terms, respectively. HLN equation best describes the competition between spin-orbit coupling and weak localization. MC behaviour in LP/HP-LMO-SIO is in good agreement with the HLN model in the temperature range between 5 K and 100 K. We could extract different scattering parameters as a function of temperature, as shown in Fig. 2a-c. The magnitude of these parameters obtained for our samples is one order of magnitude higher in comparison to the direct SrIrO₃ layer grown on LSAT with similar deposition conditions.

The elastic scattering field (B_e) which is one order of magnitude higher compared to B_i and B_{so} fields which are in agreement with the fact that the electronic transport is dominated by two-dimensional (2D) weak localization [36]. We could see that the parameter B_i has comparable magnitudes in both LP-/HP- LMO-SIO samples and follows a similar temperature dependent trend. However, HP-LMO-SIO has higher B_e values compared to the LP-LMO-SIO, which agrees with the interaction of conduction electrons in SrIrO₃ with the magnetic moment of interfacial Mn spins. In HP-LMO-SIO the magnetic moment is higher compared to LP-LMO-SIO, hence the

higher magnitude of B_e in the HP-LMO-SIO sample can be attributed to electrons screened due to interfacial Mn spins.

In the case of B_{so} , both samples exhibit different behaviour as function of temperature, and the LP-LMO-SIO show a decrease in B_{so} and saturates above 25 K. Whereas the B_{so} parameter increases till 25 K and saturates afterwards for the HP-LMO-SIO. The magnitude of B_{so} is one order higher compared to SrIrO₃ directly grown on LSAT. The B_{so} parameter is directly related to the induced spin-orbit coupling at the SrIrO₃ layer. Therefore, the temperature-dependent trend of B_{so} and B_e parameters point to the fact that the Mn spins at the interface and their magnetic moment plays a vital role in tuning the spin-orbit coupling at the interface.

The role of Mn spins on the scattering of electrons at the interface could be arising from an internal electric field generated due to charge transfer from Ir ions to Mn ions. Recent report of Huang *et al.* on LaMnO₃/SrIrO₃ superlattices showed the internal electric field arising from the strain induced in the Ir-O-Ir bond angle, which is having a Rashba-like character, at the LaMnO₃-SrIrO₃ interface [37]. Rashba interactions caused by broken mirror symmetry, and in particular by the associated electric field perpendicular to the SrIrO₃ interface induces orbital and lattice polarization due to asymmetric inter-

facial structure of LaMnO₃-SrIrO₃ interface [37]. The temperature-dependent Rashba spin-orbit coupling has earlier studied in several semiconductor heterostructures [38]. The higher-order terms in Rashba spin-orbit Hamiltonian is found to be origin of this temperature dependence [39]. In case of SrIrO₃, temperature dependence of Rashba spin-orbit coupling is reported to arise from changes in Land g factor which is affected by temperature [33]. To investigate the role of Rashba spin-orbit coupling in magnetotransport at the LaMnO₃-SrIrO₃ interface, the Rashba coefficients for LP-/HP- LMO-SIO were obtained as a function of temperature from B_{so} parameter. The B_{so} parameter is related to the Rashba spin-orbit coupling coefficient as,[33, 40, 41]

$$\alpha = \frac{(e\hbar^3 B_{so})^{\frac{1}{2}}}{m_*} \quad (2)$$

Here m^* is the effective mass, in case of SrIrO₃ $m^* \sim 7m_o$ (m_o : the mass of an electron) [33, 40] e is the elementary charge and \hbar is the reduced Plancks constant. The Rashba spin-orbit coupling coefficients (α ; eVpm) are plotted as a function of temperature for both samples, as shown in Fig. 2d. The value of α has been obtained for SrIrO₃ thin films grown on compressively strained LSAT (001) and STO (001) substrate by Zhang *et al.* [33], which exactly matches with the single SrIrO₃ layer grown on LSAT substrates. In both LP-/HP- LMO-SIO samples, the Rashba spin-orbit coupling coefficient is found to be even higher, with a 10% increase compared to SrIrO₃ directly grown on LSAT substrates. This enhanced Rashba spin-orbit coupling is due to charge transfer, depending on the valence state of underlying Mn, which shows different temperature dependence at low temperatures. Moreover, HP-LMO-SIO shows a weak temperature dependence compared to LP-LMO-SIO at low temperatures though both saturates at high temperatures (above 25 K). The interfacial coupling between different magnetically ordered LaMnO₃ also provides an impact on the coupling between the spin-orbit coupled state of Ir⁴⁺. As we know, changing the growth pressure on LaMnO₃ significantly affects the lattice constant of LaMnO₃ layer [20]. LaMnO₃ grown under low pO_2 were partially relaxed with the lattice constant $a_{LP} = 0.400$ nm. On the other hand, for thin films grown under oxidizing atmospheres are found to be compressively strained (-0.63%), with lattice constant $a_{HP} = 0.392$ nm (shown in supplementary Figure S3). It has been found that SrIrO₃ grown on LaMnO₃ is strained due to the strain in LaMnO₃ lattice. This may lead to change in Ir-O-Ir bond angle (lattice polarization). The IrO₆ octahedral rotation due to strain in the Ir-O-Ir bond angle has also been found to enhance interfacial charge transfer[28], that may enhance the electric field responsible for Rashba spin-orbit coupling.

To get more insights about the influence of interface induced Rashba spin-orbit coupling in spin relaxation mechanism in these bilayers, we considered two com-

monly observed mechanisms: the Dyakonov-Perel (DP) and the Elliot-Yafet (EY) mechanisms [42]. The DP type spin relaxation arises in systems that lack inversion symmetry, in which the electron spin precesses in an effective magnetic field with its direction changing after each scattering event [43, 44]. Depending on whether it is bulk or interface, the DP mechanism has Dresselhaus and Rashba type contributions respectively [45, 46]. On the other hand, the EY mechanism originates from spin-orbit coupling induced spin dephasing due to electron-phonon coupling or interfacial defects [42]. Apart from this in thin films, there could be other contributions to EY mechanism such as scattering events at the grain boundary, oxygen vacancy induced defects and lattice dislocations [47, 48]. Both DP and EY mechanisms can be identified by the relation between spin scattering timescale τ_{so} and momentum scattering timescale τ_p . If the τ_{so} scales linearly with τ_p then the dominant mechanism is EY, and if it is inversely proportional, the DP type is the dominant mechanism [42]. The magnitudes of τ_{so} will be greater than τ_p in semiconducting systems where the spin orbit coupling is usually weak which results in EY mechanism[42]. This is in contrast with materials with large spin-orbit coupling like Au, where the magnitudes of τ_{so} and τ_p are comparable [49]. A recent theoretical report by Kiss *et al.* with a generalized theory of EY mechanism in materials with large spin-orbit coupling argues that if the spin-orbit coupling energy (ξ) is comparable with the coulombic correlation energy (U), the τ_p values can approach τ_{so} values [50].

In HP- and LP- LMO-SIO samples the spin relaxation timescale τ_{so} and momentum relaxation (τ_p) timescale were estimated from B_{so} and B_e fields respectively through,[42]

$$\tau_{so} = \frac{\hbar}{4eB_{so}D} \quad (3a)$$

$$\tau_p = \frac{\hbar}{4eB_eD} \quad (3b)$$

Here D is the diffusion coefficient, which is calculated from the mobility deduced from Kohlers equation near small magnetic fields [51, 52]. To investigate the correlations between τ_{so} and τ_p in the HP- and LP- LMO-SIO samples, τ_{so} and τ_p with increase in temperatures are plotted in Fig. 2e. Elliott-Yafet (EY) mechanism has recently been reported as the dominant spin relaxation mechanism in SrIrO₃ thin films [53]. Here, τ_{so} is directly proportional to τ_p which shows that the dominant spin relaxation mechanism is the EY mechanism in both HP-LMO-SIO and LP-LMO-SIO samples as shown in Fig. 2e. As the interface showed enhancement in Rashba spin-orbit coupling, the much-anticipated spin relaxation mechanism was DP, instead we observed a dominant EY mechanism with 100% enhanced τ_p values compared to previous reports [53]. Our observation of EY mechanism in spin relaxation and relatively higher and comparable magnitude of τ_{so} , in the LP- and HP- LMO-SIO agrees

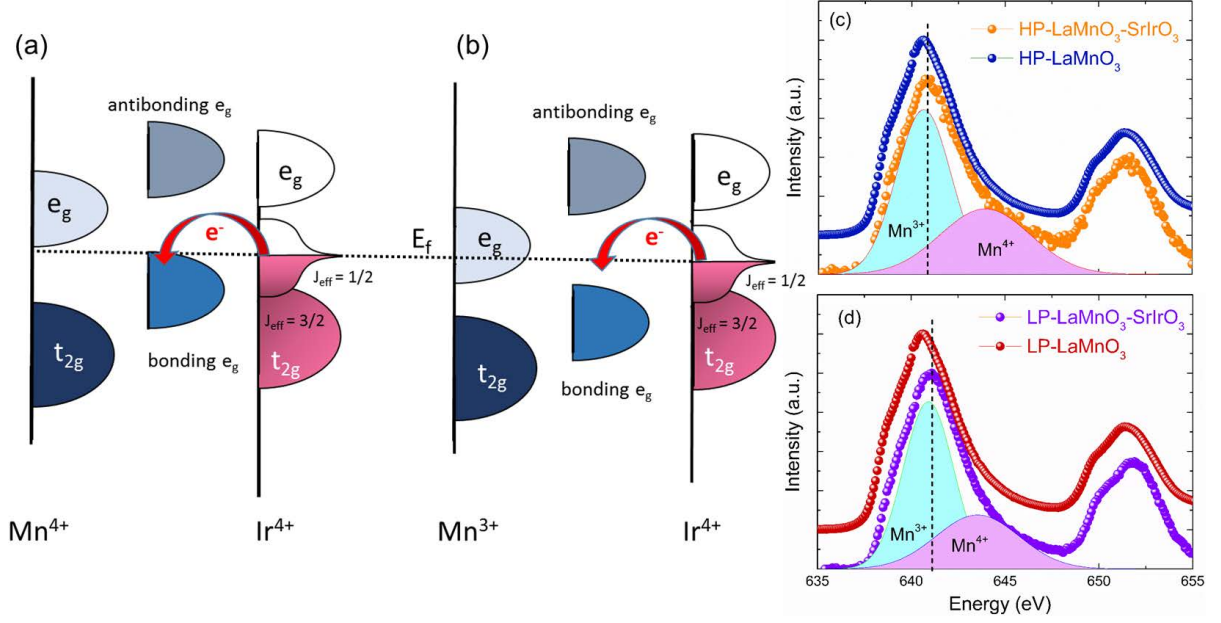


FIG. 3. Schematic representation of charge transfer mechanism for Ir^{4+} to Mn^{4+} (panel a) and Ir^{4+} to Mn^{3+} (panel b). (c) and (d) XAS spectra around Mn $L_{2,3}$ edge of HP- and LP- LMO-SIO samples along with corresponding HP- and LP- LMO samples without SrIrO_3 layer. The respective Mn valence state position, as deconvoluted Mn L - 3 edge is shown for Mn^{3+} and Mn^{4+} in the bilayer as a shaded area (valence states are quantified by XPS spectra analysis (see supplementary Fig. S4), the shaded area is for representation). The dashed black lines in the figure are guide to the eye based on the shift of the Mn- L edge position of LP- and HP- LMO-SIO with their corresponding LaMnO_3 samples.

with theoretical report of the Kiss *et al.* on the role of spin-orbit coupling in enhanced and comparable relaxation time scales in the EY mechanism in strongly correlated systems[50]. Though the magnitude of Rashba spin-orbit coupling is higher in the LaMnO_3 - SrIrO_3 interface, contribution from DP mechanism might get suppressed due to the large spin-orbit coupling. The charge transfer induced electric field may induce scattering centers resulting in an EY type spin relaxation mechanism. The fact that the slope of τ_{so} vs τ_p plot (Fig. 2e) for HP-LMO-SIO sample is higher compared to the LP-LMO-SIO sample underlines the above argument, this also reaffirms the relatively higher contribution of spin-flip scattering at the interface due to higher magnitude of HP-LMO-SIO magnetic moment. The enhanced magnitudes of τ_{so} and τ_p is related to the interfacial modifications induced spin-orbit coupling interactions, which needs to be understood further in terms of charge transfer effects.

In the case of bulk LaMnO_3 , under the crystal field created by oxygen 2p states in octahedrally coordinated MnO_6 , the five Mn $3d$ levels split into low-energy t_{2g}

triplet and high-energy e_g doublet levels, as sketched in Fig. 3a and b. In general, in hole-doped LaMnO_3 systems, the Mn ions are in a mixed trivalent ($3d^4$) and tetravalent ($3d^3$) states [29]. In the case of Mn^{4+} the e_g orbitals are empty and singly occupied for Mn^{3+} . In our case, we have mixed-valence states with varying amount of Mn^{3+} and Mn^{4+} for HP- and LP- LMO-SIO samples. Further, the e_g states of Mn^{3+} and Mn^{4+} couples with interfacial e_g states of Ir^{4+} to give rise to molecular orbitals with energetically lower lying bonding and upper lying antibonding levels [29]. This coupling of $e_g(3z^2-r^2)$ bonding orbital states at the interface promotes charge transfer from Ir^{4+} to Mn^{3+} and Mn^{4+} states. To experimentally ascertain the charge transfer at the interface, X-ray absorption spectroscopy (XAS) study in total-electron-yield (TEY) mode has been performed on HP- and LP-LMO-SIO bilayer samples and, HP- and LP-LMO without SrIrO_3 layer as illustrated in Fig. 3c and d. At first, XAS data rules out the existence of any other valence states other than Mn^{3+} and Mn^{4+} in LaMnO_3 . The LP-LMO-SIO bilayer sample shows a shift of 1.54 eV towards

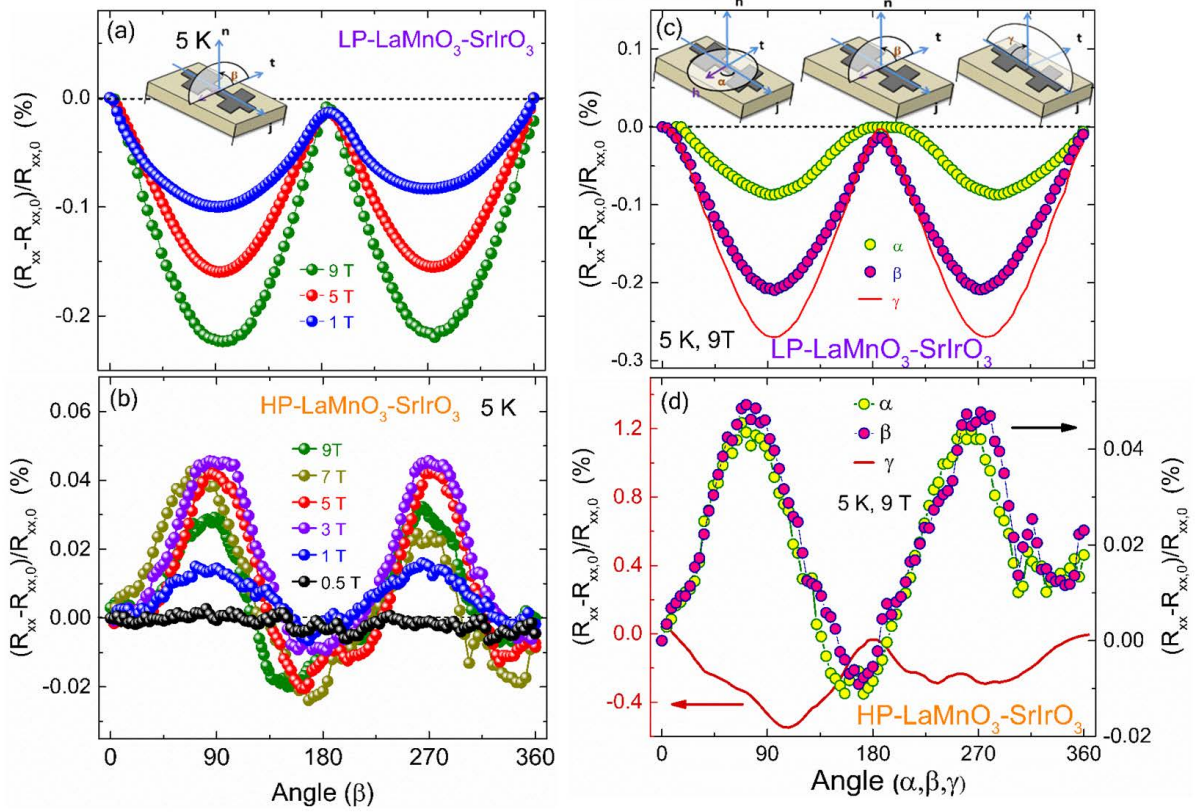


FIG. 4. (a) and (b) The angle-dependent magnetoresistance (ADMR) measurements carried out as a function of the magnetic field for LP- and HP- LMO-SIO samples respectively in β rotational plane (Schematic of the β rotational measurement configuration in inset). Figures (c) and (d) ADMR measurements as a function of different rotational configurations. The rotational planes are shown as an inset in (c). The angles α, β, γ are defined as the angle subtended between the current direction j with respect to the magnetic field rotation, and n is represented as a direction cosine normal to the surface. α points to the in-plane (IP) rotation of magnetic field with respect to n . β represent out of plane (OOP) rotation direction lying in the plane perpendicular to the current direction j . γ shows the OOP direction with respect to the current direction plane j .

higher energy compared to LP-LMO and similarly HP-LMO-SIO shows a shift of 0.25 eV compared to HP-LMO. The LP-LMO-SIO sample shows a pronounced shift due to a predominant concentration of Mn^{3+} ions over Mn^{4+} ions as seen in XPS spectra (see Figure S5). Since the Mn^{3+} bonding orbital lies much lower to the Fermi level compared to Mn^{4+} (sketched in Figure 3a and 3b) the Mn^{3+} contributes predominantly to the charge transfer process, this observation is in compliance with recently reported $\text{LaMnO}_3/\text{SrIrO}_3$ superlattices [37]. Also the charge transfer has two competing contributions arising from strain in IrO_6 octahedra and due to overlap of low lying e_g bonding orbitals in Mn^{3+} compared to Mn^{4+} at the interface. Our data shows the charge transfer being responsible for EY type spin relaxation mechanism in LMO-SIO interface. However, it is still necessary to use other complimentary experimental methods to understand further the variation in Land g-factor of SrIrO_3 in LP-/HP- LMO-SIO heterostructures as a function of temperature.

We have further carried out angle-dependent magnetoresistance (ADMR) measurements to understand the charge transfer effects on transport behaviour in SrIrO_3 due to the interfacial Mn spins in HP- and LP-LMO-SIO samples. The $\text{ADMR}(\%) = [R(\alpha, \beta, \gamma) - R(0)]/R(0)$ investigated as a function of magnetic field and rotational planes at 5 K, where $R(0)$ is the resistance when magnetic field is normal to sample surface and $R(\alpha, \beta, \gamma)$ is the resistance with respect to each rotational plane (α, β, γ) as shown in the Figure 4c inset. We observed ADMR signals with a phase shift for LP-LMO-SIO compared to HP-LMO-SIO sample. In particular, we observe a distinct magnetoresistance trend in LP-LMO-SIO sample as $[\text{MR}(\gamma) > \text{MR}(\beta) \gg \text{MR}(\alpha)]$ (Fig.4c) compared to spin Hall magnetoresistance (SMR) which has the form $[\text{MR}(\alpha) = \text{MR}(\beta) \gg \text{MR}(\gamma)]$. This ADMR trend of LP-LMO-SIO does not comply with the conditions meant for anisotropic magnetoresistance (AMR), *i.e.* $[\text{MR}(\alpha) = \text{MR}(\gamma) \gg \text{MR}(\beta)]$. This is also distinct from the recently reported proximity induced magnetoresistance (PMR) for

which the condition is $[\text{MR}(\beta) = \text{MR}(\gamma) \gg \text{MR}(\alpha)]$ [54]. On the other hand, in the case of the HP-LMO-SIO the trend points to $[\text{MR}(\gamma) > \text{MR}(\beta) = \text{MR}(\alpha)]$ (Fig.4d), this does not resemble to any above mentioned magnetoresistance models. Additionally, the observed ADMR data is quite different from reported MPE (magnetic proximity effect) in SMR of ferromagnets (FM)[55] and MPE in SMR of antiferromagnets (AFM) [56].

LaMnO₃ orients as an A-type antiferromagnet in bulk and thin films, as shown in earlier reports using scanning SQUID microscopy [19]. In the case of fully relaxed LaMnO₃ thin films, the intra-plane exchange interaction is ferromagnetic, whereas the inter-plane exchange interaction is antiferromagnetic, which may lead to an A-type antiferromagnetic ordering. However, in our case we have strained epitaxial films, that have ferromagnetic exchange interactions that results in overall ferromagnetic ordering. In LP-LMO-SIO samples, we expect the overall magnetic ordering is antiferromagnetic and the trend and magnitude of ADMR correspond to the effect of induced magnetism at the interface, such that magnetization rotation is reflected in the ADMR data. This observation were in agreement with the field-dependent changes in ADMR signals of LP-/HP- LMO-SIO samples. In the case of LaMnO₃-SrIrO₃ bilayers, there is a mixed effect from SMR as well as proximity-induced magnetism (MPE) arising from charge transfer at the interface. The field-dependent ADMR (Fig. 4a and b) in HP-LMO-SIO sample show an amplified signal at 3 T, and it decreases with increasing magnetic field strength, which suggests the existence of competing domains which percolates with increasing magnetic field in LaMnO₃. In the LP-LMO-SIO sample case, we have observed a non-saturating ADMR which is due to the presence of antiferromagnetic order that prevails with the magnetic field and MPE being a dominant contribution arising from induced magnetism in LaMnO₃-SrIrO₃ interface. Further experimental and theoretical studies are required to understand the domain structure of LaMnO₃ with MPE effects, to extract the spin-charge conversion at LaMnO₃-SrIrO₃ interface using a theoretical macrospin model to explore such a complicated magnetic structure.

III. CONCLUSION

In summary, we have explored the *3d-5d* interface interactions through tunability of the magnetic order in LaMnO₃ by varying the oxygen partial pressure during LaMnO₃ deposition. The X-ray spectroscopy measurements indicate the changes in the magnetic ordering of

LaMnO₃ can be attributed to the creation of multiple valence states. A tunable and enhanced Rashba spin-orbit coupling is estimated at LP- and HP-LMO-SIO as a function of temperature from magnetoconductance measurements that arises from electric field generated due to strain in Ir-O-Ir bond angle as well as interfacial charge transfer from Ir⁴⁺ to Mn³⁺ and Mn⁴⁺. The spin relaxation mechanism at LaMnO₃-SrIrO₃ interface is observed to follow the Elliott-Yafet mechanism. The spin relaxation parameters are in agreement with the generalized theory of EY mechanism for materials with large spin-orbit coupling. The contribution of Mn spins in LaMnO₃ on electronic transport was further probed using ADMR measurements, which reflects the magnetic order of underlying LaMnO₃ and charge transfer induced magnetism at LaMnO₃-SrIrO₃ interface. The evolution of these phenomena is attributed to the *3d-5d* interface electronic correlation and the Rashba spin-orbit coupling at the LaMnO₃-SrIrO₃ interface. In conclusion, the present results provide a novel platform of *3d-5d* oxide interface engineering and raises possibilities in tuning these interface interactions to optimize spin transport in emerging quantum material SrIrO₃.

ACKNOWLEDGMENTS

M.S.R. and K.S would like to acknowledge the SERBDST Extra Mural Funding for the purchase of a horizontal rotating holder (Quantum Design) from the project EMR/2017/002328. The authors would like to acknowledge Dr. Matthias Opel and Dr. Matthias Althammer of Walther Meissner Institute Garching, Technical University of Munich (TUM) Germany for insightful discussions and suggestions in the modification of the manuscript. The authors would like to acknowledge Professor Mahendran and his student Amit Chanda of National University of Singapore (NUS) for their help in measurements. This work was financially supported by the SERB-DST (EMR/2017/002328). The research at NUS is supported by the Agency for Science, Technology and Research (A*STAR) under its Advanced Manufacturing and Engineering (AME) Individual Research Grant (IRG) (A1983c0034), the National University of Singapore (NUS) Academic Research Fund (AcRF Tier 1 Grant No. R-144-000-391-144 and R-144-000-403-114) and the Singapore National Research Foundation (NRF) under the Competitive Research Programs (CRP Award No. NRF-CRP15-2015-01). H.J. would like to thank NUS Graduate School of Integrative Science and Engineering (NGS) for fellowship.

[1] J. Nichols, X. Gao, S. Lee, T. L. Meyer, J. W. Freeland, V. Lauter, D. Yi, J. Liu, D. Haskel, J. R. Petrie, E.-J. Guo, A. Herklotz, D. Lee, T. Z. Ward, G. Eres, M. R. Fitzsimmons, and H. N. Lee, Nature Communications **7**,

12721 (2016).

[2] A. Ohtomo and H. Hwang, Nature **427**, 423 (2004).

[3] K. S. Takahashi, M. Kawasaki, and Y. Tokura, Applied Physics Letters **79**, 1324 (2001).

- [4] C. Cen, S. Thiel, G. Hammerl, C. W. Schneider, K. E. Andersen, C. S. Hellberg, J. Mannhart, and J. Levy, *Nature Materials* **7**, 298 (2008).
- [5] J. Hoffman, I. C. Tung, B. B. Nelson-Cheeseman, M. Liu, J. W. Freeland, and A. Bhattacharya, *Phys. Rev. B* **88**, 144411 (2013).
- [6] A. Manchon, H. C. Koo, J. Nitta, S. M. Frolov, and R. A. Duine, *Nature Materials* **14**, 871 (2015).
- [7] A. Soumyanarayanan, N. Reyren, A. Fert, and C. Panagopoulos, *Nature* **539**, 509 (2016).
- [8] Y. A. Bychkov and E. I. Rashba, *Journal of Physics C Solid State Physics* **17**, 6039 (1984).
- [9] H. Watanabe, T. Shirakawa, and S. Yunoki, *Phys. Rev. Lett.* **105**, 216410 (2010).
- [10] T. Takayama, A. N. Yaresko, and H. Takagi, *Journal of Physics: Condensed Matter* **31**, 074001 (2018).
- [11] W. Witczak-Krempa, G. Chen, Y. B. Kim, and L. Balents, *Annual Review of Condensed Matter Physics* **5**, 5782 (2014).
- [12] B. J. Kim, H. Ohsumi, T. Komesu, S. Sakai, T. Morita, H. Takagi, and T. Arima, *Science* **323**, 1329 (2009).
- [13] A. Biswas, K.-S. Kim, and Y. H. Jeong, *Journal of Applied Physics* **116**, 213704 (2014).
- [14] A. Biswas and Y. H. Jeong, *Current Applied Physics* **17**, 605 (2017), oxide Heterostructure Research in Korea.
- [15] A. Biswas, K.-S. Kim, and Y. H. Jeong, *Journal of Magnetism and Magnetic Materials* **400**, 36 (2016), proceedings of the 20th International Conference on Magnetism (Barcelona) 5-10 July 2015.
- [16] J. Tpfers and J. Goodenough, *Journal of Solid State Chemistry* **130**, 117 (1997).
- [17] Q. Huang, A. Santoro, J. W. Lynn, R. W. Erwin, J. A. Borchers, J. L. Peng, and R. L. Greene, *Phys. Rev. B* **55**, 14987 (1997).
- [18] C. Ritter, M. R. Ibarra, J. M. De Teresa, P. A. Algarabel, C. Marquina, J. Blasco, J. García, S. Oseroff, and S.-W. Cheong, *Phys. Rev. B* **56**, 8902 (1997).
- [19] X. R. Wang, C. J. Li, W. M. Lü, T. R. Paudel, D. P. Leusink, M. Hoek, N. Poccia, A. Vailionis, T. Venkatesan, J. M. D. Coey, E. Y. Tsymbal, Ariando, and H. Hilgenkamp, *Science* **349**, 716 (2015).
- [20] J. Roqueta, A. Pomar, L. Balcells, C. Frontera, S. Valencia, R. Abrudan, B. Bozzo, Z. Konstantinovi, J. Santiso, and B. Martinez, *Crystal Growth & Design* **15**, 5332 (2015).
- [21] L. Wu, C. Li, M. Chen, Y. Zhang, K. Han, S. Zeng, X. Liu, J. Ma, C. Liu, J. Chen, J. Zhang, Ariando, T. V. Venkatesan, S. J. Pennycook, J. M. D. Coey, L. Shen, J. Ma, X. R. Wang, and C.-W. Nan, *ACS Applied Materials & Interfaces* **9**, 44931 (2017), pMID: 29236463.
- [22] A. M. Zhang, W. C. Zhang, X. S. Wu, and J. G. Lin, *AIP Advances* **7**, 055837 (2017).
- [23] I. Marozau, P. T. Das, M. Döbeli, J. G. Storey, M. A. Uribe-Laverde, S. Das, C. Wang, M. Rössle, and C. Bernhard, *Phys. Rev. B* **89**, 174422 (2014).
- [24] X. Liu, M. Kotiuga, H.-S. Kim, A. T. N'Diaye, Y. Choi, Q. Zhang, Y. Cao, M. Kareev, F. Wen, B. Pal, J. W. Freeland, L. Gu, D. Haskel, P. Shafer, E. Arenholz, K. Haule, D. Vanderbilt, K. M. Rabe, and J. Chakhalian, *Proceedings of the National Academy of Sciences* **116**, 19863 (2019).
- [25] D. Yi, C. L. Flint, P. P. Balakrishnan, K. Mahalingam, B. Urwin, A. Vailionis, A. T. N'Diaye, P. Shafer, E. Arenholz, Y. Choi, K. H. Stone, J.-H. Chu, B. M. Howe, J. Liu, I. R. Fisher, and Y. Suzuki, *Phys. Rev. Lett.* **119**, 077201 (2017).
- [26] Y. Li, J. Zhou, and D. Wu, *ACS Applied Materials & Interfaces* **11**, 3565 (2019).
- [27] Y. Li, L. Zhang, Q. Zhang, C. Li, T. Yang, Y. Deng, L. Gu, and D. Wu, *ACS Applied Materials & Interfaces* **11**, 21268 (2019), pMID: 31117466.
- [28] S. Okamoto, J. Nichols, C. Sohn, S. Y. Kim, T. W. Noh, and H. N. Lee, *Nano Letters* **17**, 2126 (2017), pMID: 28256840.
- [29] T. Yu, B. Deng, L. Zhou, P. Chen, Q. Liu, C. Wang, X. Ning, J. Zhou, Z. Bian, Z. Luo, C. Qiu, X.-Q. Shi, and H. He, *ACS Applied Materials & Interfaces* **11**, 44837 (2019), pMID: 31680512.
- [30] M. Isasa, S. Vélez, E. Sagasta, A. Bedoya-Pinto, N. Dix, F. Sánchez, L. E. Hueso, J. Fontcuberta, and F. Casanova, *Phys. Rev. Applied* **6**, 034007 (2016).
- [31] A. Aqeel, N. Vlietstra, A. Roy, M. Mostovoy, B. J. van Wees, and T. T. M. Palstra, *Phys. Rev. B* **94**, 134418 (2016).
- [32] A. S. Patri, K. Hwang, H.-W. Lee, and Y. B. Kim, *Scientific Reports* **8**, 8052 (2018).
- [33] L. Zhang, Y. B. Chen, B. Zhang, J. Zhou, S. Zhang, Z. Gu, S. Yao, and Y. Chen, *Journal of the Physical Society of Japan* **83**, 054707 (2014).
- [34] L. Zhang, Q. Liang, Y. Xiong, B. Zhang, L. Gao, H. Li, Y. B. Chen, J. Zhou, S.-T. Zhang, Z.-B. Gu, S.-h. Yao, Z. Wang, Y. Lin, and Y.-F. Chen, *Phys. Rev. B* **91**, 035110 (2015).
- [35] S. Hikami, A. I. Larkin, and Y. Nagaoka, *Progress of Theoretical Physics* **63**, 707 (1980).
- [36] M. Pollak and B. Shklovskii, *Hopping Transport in Solids*. (Elsevier Science, Amsterdam, 2014) oCLC: 1058710254.
- [37] K. Huang, L. Wu, M. Wang, N. Swain, M. Motapothula, Y. Luo, K. Han, M. Chen, C. Ye, A. J. Yang, H. Xu, D.-c. Qi, A. T. N'Diaye, C. Panagopoulos, D. Primetzhofer, L. Shen, P. Sengupta, J. Ma, Z. Feng, C.-W. Nan, and X. Renshaw Wang, *Applied Physics Reviews* **7**, 011401 (2020).
- [38] M. A. Leontiadou, K. L. Litvinenko, A. M. Gilbertson, C. R. Pidgeon, W. R. Branford, L. F. Cohen, M. Fearn, T. Ashley, M. T. Emeny, B. N. Murdin, and S. K. Clowes, *Journal of Physics: Condensed Matter* **23**, 035801 (2011).
- [39] P. S. Eldridge, W. J. H. Leyland, P. G. Lagoudakis, O. Z. Karimov, M. Henini, D. Taylor, R. T. Phillips, and R. T. Harley, *Phys. Rev. B* **77**, 125344 (2008).
- [40] D. N. Basov, R. D. Averitt, D. van der Marel, M. Dressel, and K. Haule, *Rev. Mod. Phys.* **83**, 471 (2011).
- [41] C. Schierholz, T. Matsuyama, U. Merkt, and G. Meier, *Phys. Rev. B* **70**, 233311 (2004).
- [42] I. Žutić, J. Fabian, and S. Das Sarma, *Rev. Mod. Phys.* **76**, 323 (2004).
- [43] M. I. D'yakonov, *Sov. Phys. JETP* **33**, 1053 (1971).
- [44] M. I. D'yakonov, *Sov. Phys. Semicond.* **20**, 110 (1986).
- [45] P. D. Dresselhaus, C. M. A. Papavassiliou, R. G. Wheeler, and R. N. Sacks, *Phys. Rev. Lett.* **68**, 106 (1992).
- [46] A. D. Caviglia, M. Gabay, S. Gariglio, N. Reyren, C. Cancellieri, and J.-M. Triscone, *Phys. Rev. Lett.* **104**, 126803 (2010).
- [47] R. J. Elliott, *Phys. Rev.* **96**, 266 (1954).
- [48] F. Seitz and D. Turnbull, *Solid state physics: advances in research and applications. Volume 14* Volume 14 (Aca-

- demic Press, New York, 1963) oCLC: 646774983.
- [49] P. Monod and F. Beuneu, Phys. Rev. B **19**, 911 (1979).
 - [50] A. Kiss, L. Szolnoki, and F. Simon, Scientific Reports **6**, 22706 (2016).
 - [51] J. L. Olsen, *Electron transport in metals* (Interscience Publishers, New York, 1962).
 - [52] H. Li, H. He, H.-Z. Lu, H. Zhang, H. Liu, R. Ma, Z. Fan, S.-Q. Shen, and J. Wang, Nature Communications **7**, 10301 (2016).
 - [53] L. Zhang, X. Jiang, X. Xu, and X. hao Hong (2019) arXiv:1907.11814v1.
 - [54] K. Takiguchi, L. Duc Anh, T. Chiba, T. Koyama, D. Chiba, and M. Tanaka, Nature Physics **15** (2019).
 - [55] X. Zhou, L. Ma, Z. Shi, W. J. Fan, J.-G. Zheng, R. F. L. Evans, and S. M. Zhou, Phys. Rev. B **92**, 060402 (2015).
 - [56] Y. Cheng, S. Yu, A. S. Ahmed, M. Zhu, Y. Rao, M. Ghazisaeidi, J. Hwang, and F. Yang, Phys. Rev. B **100**, 220408 (2019).